LHCb Collaboration

LHCb 2001-040 VELO
21st May 2001

Performance of an irradiated *p*–on–*n* MICRON prototype VELO detector

T. Bowcock [1] J. Buytaert [2] G. Casse [1] M. Charles [3] H. Dijkstra [2] P. Collins [2] O. Dormond [4] M. Ferro-Luzzi [2] F. Fiedler [2] R. Frei [4] G. Gagliardi [4] P. Jalocha [5] J. Libby [2] T. Ketel [6] C. Parkes [1] U. Parzefall [1] T. Ruf [2] M. Tareb [4] F. Teubert [2] V. Wright [1] M. Witek [5]

Abstract

A 200 μm thick *p*–on–*n* design LHCb PR-02 prototype VELO detector was irradiated and equipped with LHC–speed electronics. This detector was successfully operated in a test–beam and its performance assessed.

After an irradiation dose corresponding to between one and two years of LHCb operation the depletion voltage was found to be 320 V, significantly greater than that predicted. The signal–to–noise, at full charge collection efficiency, was found to be 15. The maximum irradiation received was 10^{15} protons/cm^2: even after this very high irradiation, charge was still collected albeit with reduced cluster finding efficiency.

Particular risks associated with a *p*–on–*n* fine pitch detector with a double metal layer are identified. It was shown that at underdepletion the fine pitch *p*–on–*n* detector rapidly loses efficiency due to both charge spread and charge loss to the double metal layer.

[1]University of Liverpool, Oliver Lodge Laboratory, Liverpool, England
[2]CERN, CH-1211, Geneva 23, Switzerland
[3]Department of Nuclear and Particle Physics, Oxford University, 1 Keble Road, Oxford OX1 3RH, England
[4]Institut de Physique des Hautes Energies, Batiment des Sciences Physiques, Université de Lausanne, CH-1015 Dorigny 20, Switzerland
[5]Institute of Nuclear Physics High Energy Departments, ul. Kawiory 26 A, 30-055 Kraków, Poland
[6]NIKHEF, Kruislaan 409, 1098 SJ Amsterdam, The Netherlands

1 Introduction

In August 2000 an irradiated MICRON LHCb VELO PR-02 prototype detector was operated in a test–beam of 120 GeV muons and pions at the CERN SPS. The primary goals of the test–beam were to measure the efficiency and resolution of the detector after irradiation conditions corresponding to between one and five years of operation in LHCb.

A Hamamatsu prototype detector was tested in the same set–up. Many of the details of both the analysis methods and infrastructure used in the MICRON detector tests are described in the note presenting the results of the Hamamatsu detector tests [1]. Reference to [1] is made throughout this note.

2 Detector Description

2.1 Detector design

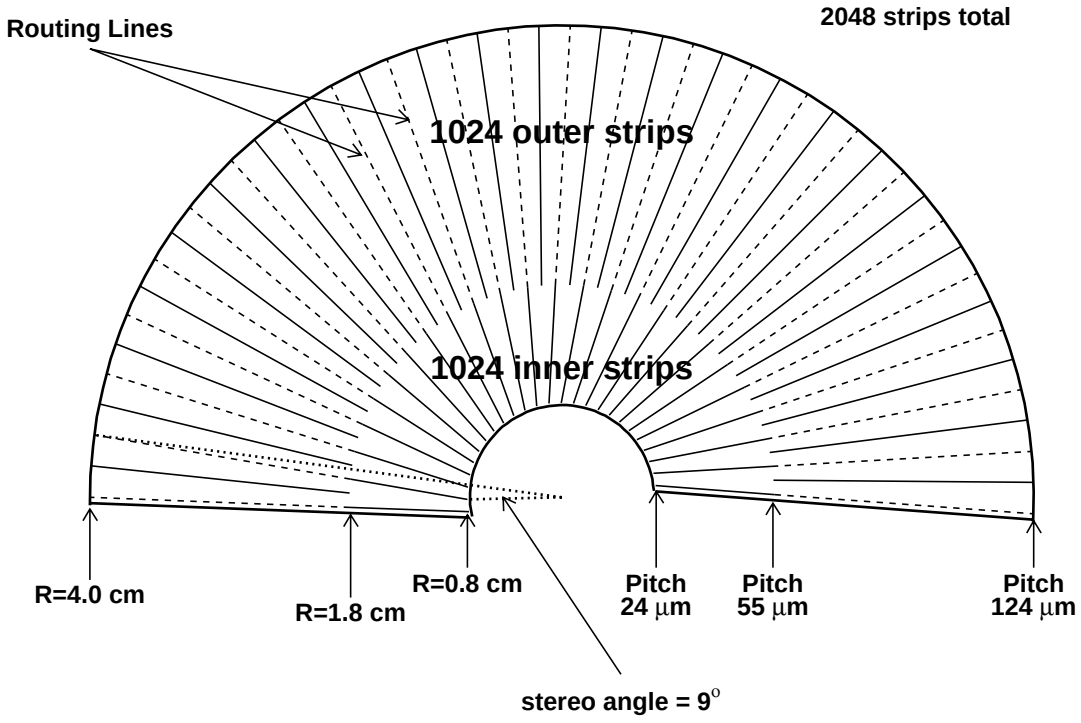

Figure 1: Strip layout of MICRON prototype ϕ (azimuthal) measuring detector.

The tested detector was a 2000 PR-02 prototype ϕ measuring detector [2] manufactured by MICRON Semiconductors[1]. The reference number of the detector is 1832–9–a [3]. The geometrical properties of the measuring sensor design are illustrated in Figure 1, further details are available in [4]. The detector contained separate strips in the inner and outer

[1] 1 Royal Buildings, Marlborough Road, Lancing, Sussex, BN15 8UN, UK.

regions. The strips ran approximately radially on the detector and hence the inter–strip pitch varied uniformly along the length of the strip. Each strip had a 9° stereo angle, which is indicated in Figure 1. The minimum pitches in the inner and outer regions were 24.4 μm and 55.5 μm respectively. The maximum radius was 4 cm and the angle covered by the detector was 182°.

The 2048 readout pads were arranged outside the outer radius of the active area of the detector. The pitch of the readout pads varied between 61.5 and 62 μm (in two staggered rows of $123 - 124$ μm). The strips from the inner region were connected to the readout pads using routing lines on a second metal layer of the detector. These routing lines ran between adjacent strips in the outer region. One pad row was used for the readout of the inner region and the other row for the outer region.

The detector was a p–on–n design with a thickness of 200 μm. No special oxygenation technique was applied to the silicon wafer.

2.2 Readout electronics

The sensor was read out using the SCT128A [5] and specially manufactured hybrids based on an ATLAS design. The hybrids were not perfectly matched to the detector, with an input pitch of 80 μm and only 3 chips per hybrid (384 channels). However, it was still possible to read out sections of the detector scanning irradiation intensities from 0 to 10^{15} protons/cm^2. The SCT128A was operated with an LHC–speed (40 MHz) clocking rate.

3 Irradiation and Annealing

3.1 Irradiation

The detector was irradiated in a 24 GeV proton beam at the CERN PS irradiation facility in July 2000. The irradiation procedure and measurement of the beam profile is described in [6]. The detector received a peak fluence of $(10.4 \pm 0.8) \times 10^{14}$ protons/cm^2. A Gaussian beam profile with a 6.1 ± 0.3 mm width was measured. A map of the irradiation profile of the detector was produced and is shown in Figure 2.

3.2 Annealing

The temperature of the detector was monitored during the irradiation procedure and prior to the collection of data in the test–beam. The temperature of the detector during all periods where it was above 0°C is shown in Figure 3(a).

A phenomenological parametrisation of the bulk radiation damage to silicon has been developed by the ROSE Collaboration [7]. The model is based on experimental results from the study of silicon diodes. Using this model, the evolution of the depletion voltage of the device has been simulated and is shown in Figure 3(b) for a range of fluences. Final depletion voltages of 419 V, 210 V and 42 V were obtained for the peak irradiation dose, 50% fluence and 10% fluence.

The final depletion voltage of the device, after type inversion, is predicted to be insensitive to the initial depletion voltage under proton irradiation. The impact of measurement errors on the temperature and time profile and the time the detector spent refrigerated

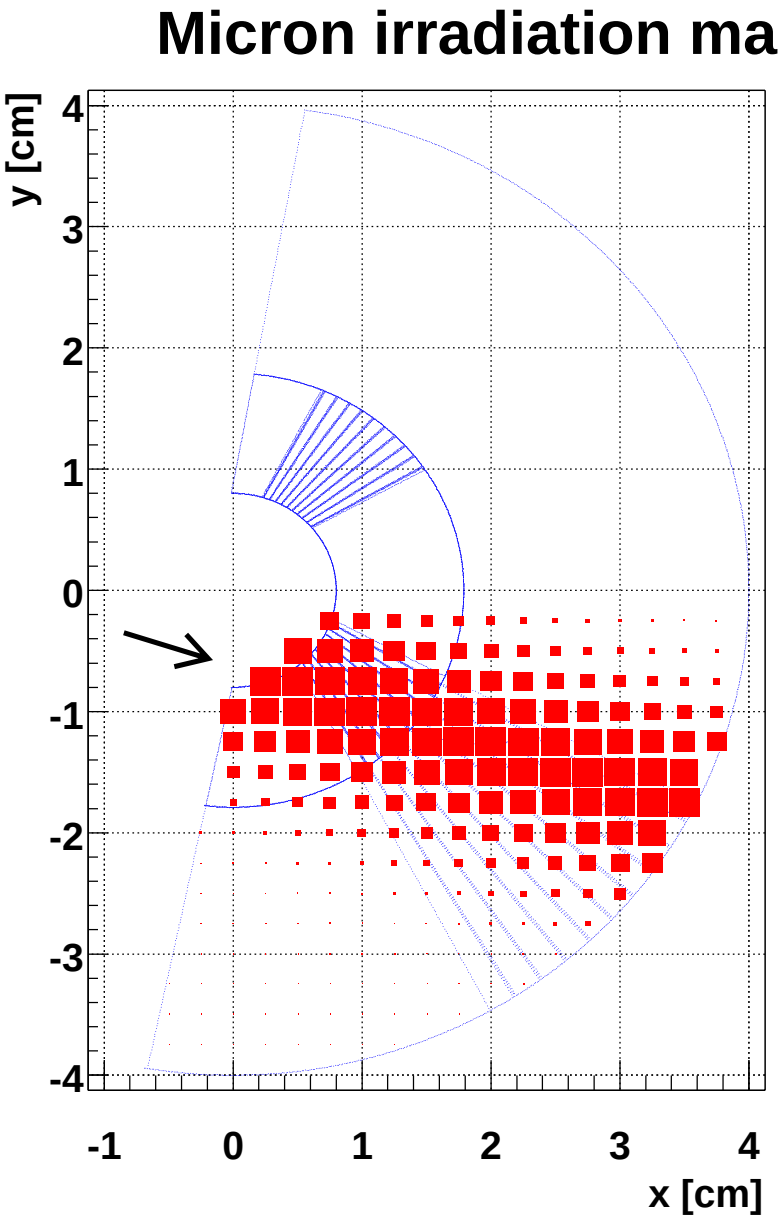

Figure 2: Positions of the instrumented regions of the MICRON detector (hatched), with the irradiation dose received at different parts of the detector superimposed. The area of the shaded squares is proportional to the irradiation dose received at that point. The arrow indicates the direction of the beam used in the irradiation.

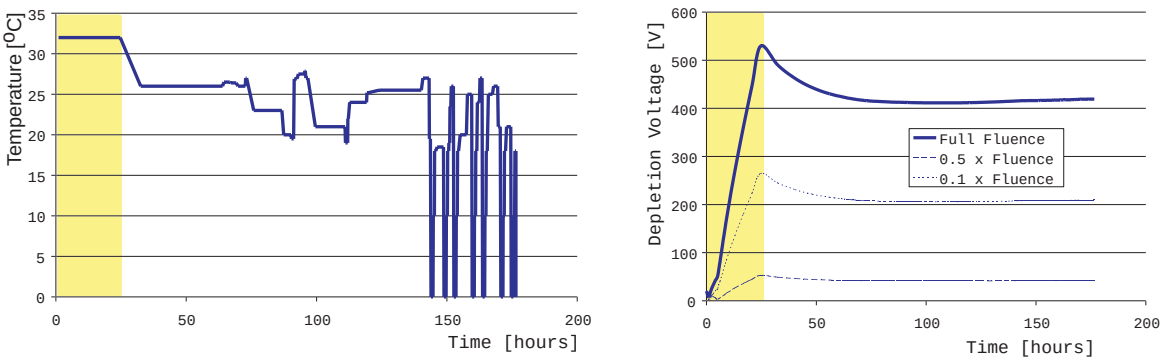

(a) (b)

Figure 3: The period that the detector spent above 0°C during and after irradiation is shown in (a). The expected depletion voltage of the sensor is shown during the same period for a range of fluences in (b). The shaded area indicates the time when the detector was being irradiated.

were found to be negligible. However, the 10% uncertainty on the irradiation fluence corresponds to a similar uncertainty on the depletion voltage. Under the same conditions the expected final depletion voltage of a neutron irradiated detector (with the equivalent dose calculated by NIEL scaling) is predicted to be about 400 V. The model predicts a very significantly improved performance for oxygenated silicon over standard silicon under proton irradiation; the final depletion voltage would be 114 V for oxygenated silicon irradiated to the same maximum level. The model parameters have a significant variation between materials, changing individual parameters by the ranges reported in [8] and its references commonly result in changes of ± 50 V. In all the scenarios considered the final depletion voltage was found to lie in a plateau close to the local minima of the curve.

4 Test–beam setup

The beam telescope is described in detail in [1]; the irradiated MICRON detector was mounted in the same insulating box described therein. The operating temperature of the detector was -12°C.

The MICRON detector was equipped for operation in the test–beam using SCT128A 3-chip hybrids. These were not perfectly matched to the pitch or geometry of the MICRON detector, and it was decided to equip two regions, corresponding to the non-irradiated and irradiated sides of the detector. Figure 4 shows a photograph of the equipped detector. The irradiated side of the detector was glued to the hybrid, and both inner and outer channels were bonded. The non-irradiated side of the detector was only fixed with heat paste, to avoid any problems arising from a difference in thermal contraction between the silicon and the aluminium support, when the set-up was cooled. Due to a leak of the heat paste it was only possible on this side to bond one row of readout pads, corresponding to the inner region. The regions read out are indicated by the shaded parts of the detector shown in Figure 2. One chip on the non–irradiated side of the detector was dead during the test–beam data taking; this chip would of read out the strips at greatest ϕ in the

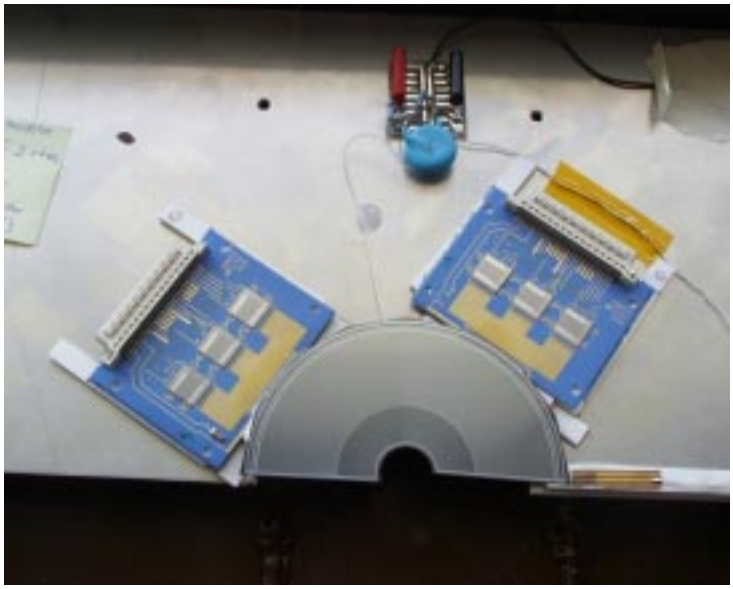

Figure 4: A photograph of the detector equipped with the readout electronics and fixed to the cooling plate.

local coordinate system of the detector. The timing and triggering of the SCT128A is described in [1].

In the test–beam the insulating box containing the MICRON detector was mounted on a support which could be moved vertically and horizontally. In this way it was possible to scan different parts of the detector with the telescope beam. Figure 5 shows the intercepts of all tracks accumulated during the test–beam with the MICRON detector, in the local detector frame. All equipped regions were covered, apart from a corner on the very large pitch region of the irradiated side. The maximum voltage put onto the detector was 390 V, following measurements of the drain current as a function of voltage carried out at Liverpool. Figure 6 shows the measured drain current as function of voltage for the MICRON detector before irradiation. The current is greater than 5 μA for voltages in excess of 350 V.

The following voltage scans were taken in different parts of the detector, as labelled in Figure 5:

- **Non-irradiated, inner region,** a single run at 300 V.
- **Irradiated, inner region,** runs were taken at 100 V, 150 V, 200 V, 250 V, 300 V, 350 V and 390 V.
- **Irradiated, outer region,** runs at 100 V, 200 V and 300 V.

5 Alignment

The alignment procedure was identical to that described in [1]. The alignment quality is illustrated in Figure 7 which shows (a) the residual distribution of width 23 μm, (b) the residuals as a function of R and (c) the residuals as a function of ϕ. The non–flat

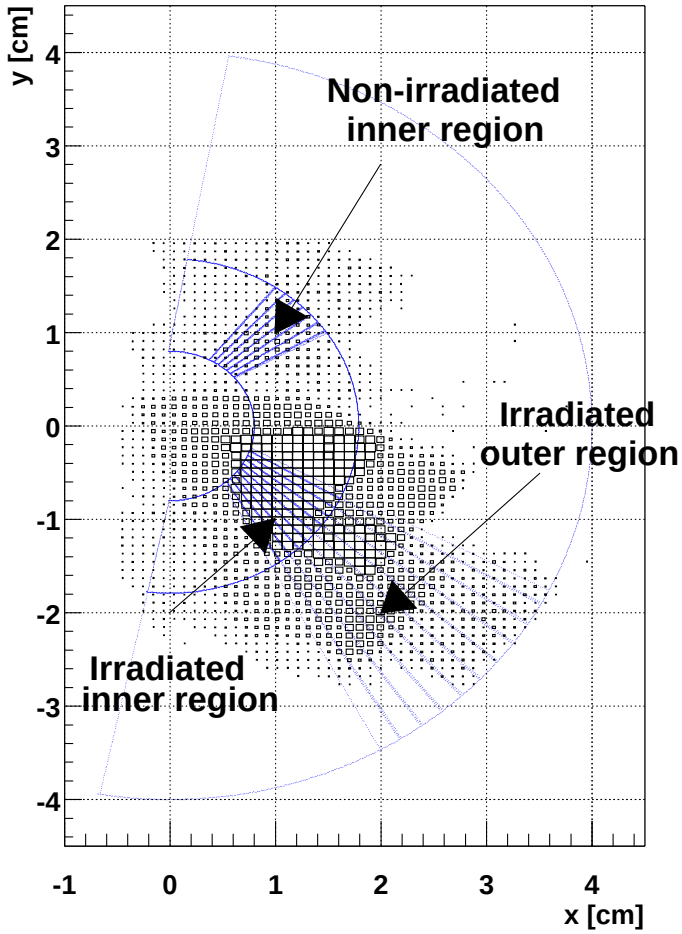

Figure 5: Intercepts of tracks in the test–beam with the MICRON detector, shown in the local MICRON detector frame, integrated over all runs.

distribution of the core of residuals as a function ϕ and R indicates that the alignment was not optimal. However, the quality is adequate for the charge collection efficiency and cluster shape analyses presented in this note.

6 Track Selection

The charge collected on the MICRON detector by a traversing track was calculated by extrapolating the telescope track to the aligned MICRON detector and summing the charge on strips adjacent to the intercept point. In order to be able to measure very low charges a cleaning procedure must be applied to the data sample, otherwise the results may be distorted by bad data or geometrical edge effects.

A set of cuts were applied to the extrapolation tracks. These were on their extrapolated fiducial position, their time with respect to the SCT128A trigger window (TDCtime) and the signal in a SCT128A equipped non–irradiated detector. The cuts applied are

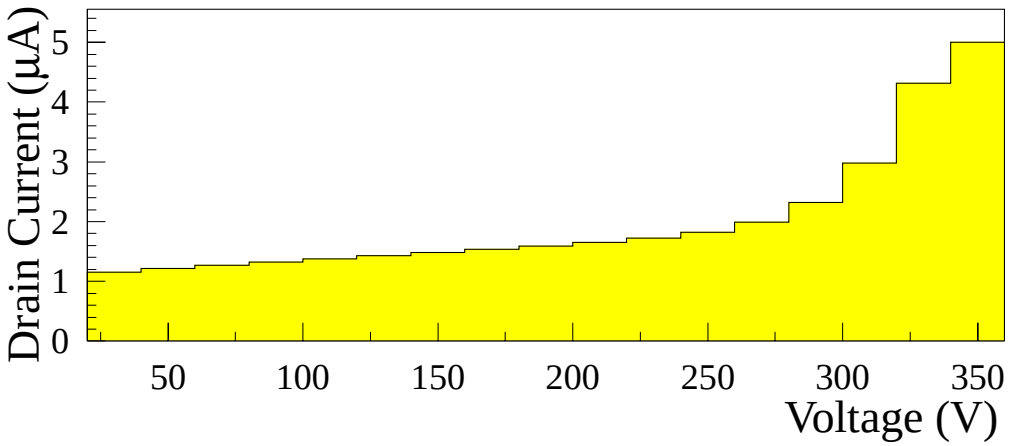

Figure 6: The drain current as function of voltage for the MICRON detector before irradiation.

Non–irradiated region	**Irradiated region**
0.85 cm $< R <$ 1.7 cm	0.85 cm $< R <$ 5 cm
0.64 rad $< \phi <$ 0.95 rad	-1.5 rad $< \phi <$ 1.5 rad
track intercepted connected strip	
0 ns $<$ TDCtime $<$ 20 ns	
signal in the fast station greater 30 ADC counts	

Table 1: The selection cuts applied to tracks intercepting the MICRON detector.

summarised in Table 1. The motivation for these cuts is described in [1].

There were a total of 43,614 tracks which traversed the equipped regions of the detector, out of a total of about 250,000 triggered events.

7 Introduction to the MICRON data and the role of the routing lines

Before the results of the charge collection efficiency (CCE), efficiency and cluster shape analyses are presented some features of the MICRON data set will be discussed in this section.

In Figure 8 the efficiency to find a cluster with a signal–to–noise of greater than 3 within 200 μm of the track intercept is shown, the details of the analysis are given in Section 9. The irradiated side is shown at three different voltages, and the non-irradiated

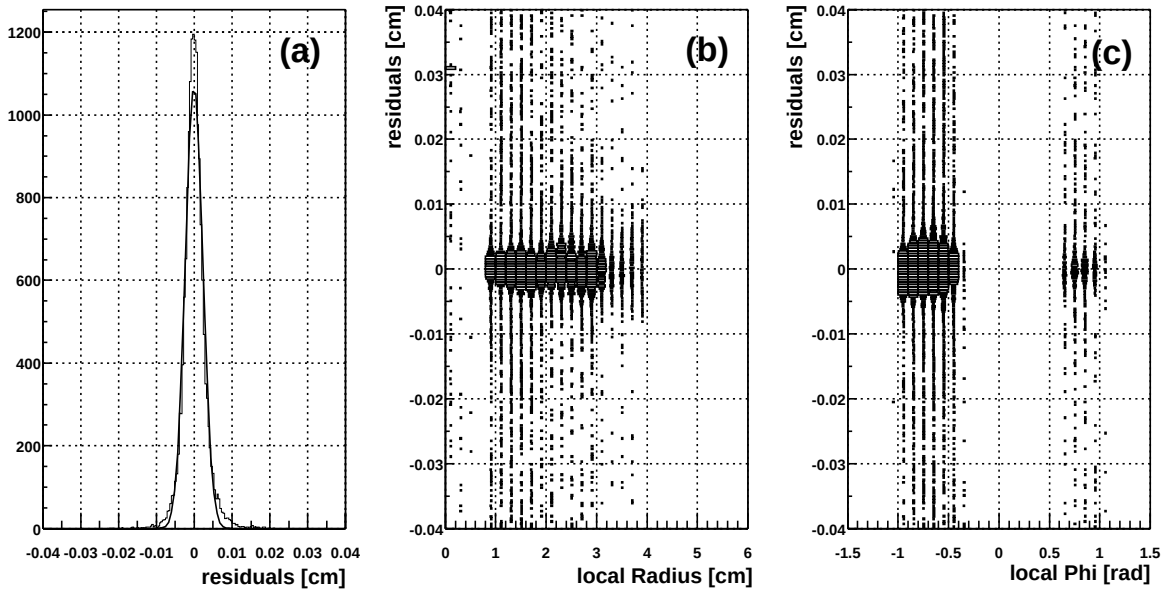

Figure 7: The quality of the MICRON detector alignment: (a) the residual distribution, (b) residuals as a function of R, and (c) residuals as a function of ϕ.

side is shown just for 300 V bias. There are two features immediately apparent from this figure:

- the damage done by the irradiation shows up as a line of inefficiency crossing the detector and,
- the outer region is clearly less efficient than the inner region at the same irradiation dose. This is due to a charge loss to the double metal layer, which occurs for underdepleted p-on-n detectors, which will be discussed in the following section.

The inner region received a quite uniform irradiation greater than 9×10^{14} protons/cm^2 over most of its area, and subsequently gives little positional information on the irradiation. In order to deduce the position of the beam, the plot of the inefficiency in the outer region was fitted in slices with a Gaussian shape. The result of this fit is shown in Figure 9(a). There is a discrepancy of $\sim 20^\circ$ between the angle measured from the data and the angle taken from the irradiation measurements [6][2]. Despite this uncertainty it can be seen in Figure 9 that the most irradiated region is still contained within the equipped part of the detector. For the measurements shown in this paper the angle measured from the data is taken as the baseline.

[2]The reason for this discrepancy is unknown, however it is suspected that MICRON detector was displaced from its nominal position in the shuttle used in the irradiation, due to insecure fastening. The problem of this fastening will be addressed in future irradiations.

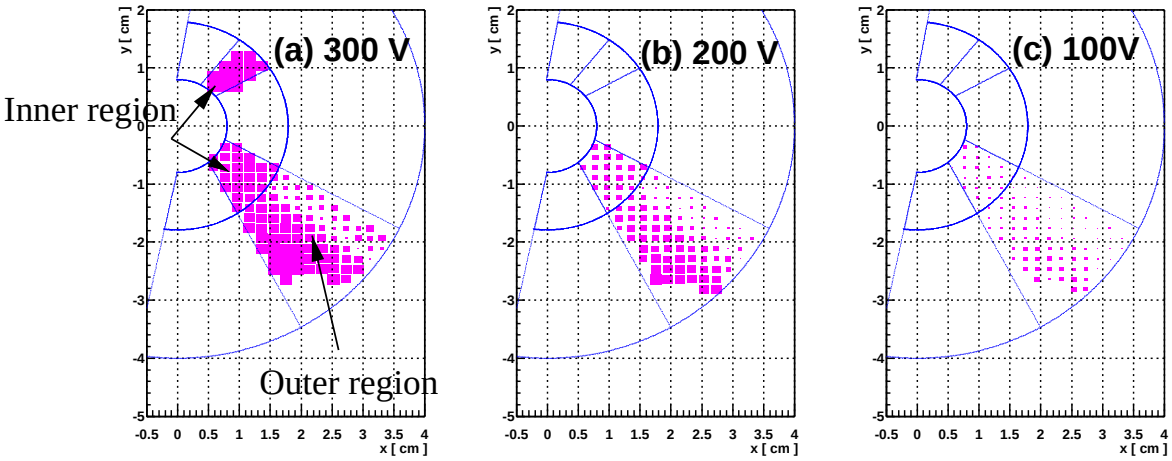

Figure 8: Efficiency measured on the MICRON detector at 3 different voltages: (a) 300 V, (b) 200 V and (c) 100 V. Data on the non–irradiated side were only collected at 300 V.

7.1 Role of the routing lines

As shown in Figure 8 there is a reduced efficiency in the outer region compared to the inner region.

The unique geometry of the MICRON ϕ measuring detector allows this effect to be fully understood. With reference to Figure 1 it can be seen that there is a fundamental difference between the inner and outer region: the outer region has routing lines between the strips and the inner does not. The inner region has diodes which are connected to these routing lines. If the charge is collected from a track passing through the inner region, the routing lines might capacitively couple to the neighbouring strips or cross–talk can take place within the readout electronics; charge would be lost in both ways. In the outer region the capacitive coupling or cross talk is the same; but, in addition it is possible to lose charge to the routing lines between strips due to a geometrical effect when the detector is underdepleted. By comparing the performance of the inner and outer regions the two effects can be deconvoluted.

The geometrical effect is illustrated in Figure 10. Part (a) shows the situation in the inner region, when the detector is fully depleted. The field lines are focused on the diodes and a narrow cluster is formed. Part (b) shows the situation in the inner region in the underdepleted case. Charges drift along the field lines, but are not focused onto the diodes, as described in [9]. This leads to an induced charge over many strips, a spread cluster, and a loss of resolution. This effect is discussed in section 10. Part (c) shows the situation in the outer region, when the detector is fully depleted. The field lines are focused on the diodes, and again a narrow cluster is seen. Part (d) shows the situation in the case of underdepletion. Again, a charge spread is seen. In addition, charge can be induced in the metal lines lying in the second metal layer. This is seen in the data as a charge loss to the routing lines. Due to the fact that the routing lines are separated from the first metal layer by a 3.8 μm thick silicon dioxide layer, less charge is seen in the routing lines than in the lines situated just over the diodes. As the routing lines are read out it is possible to measure how much charge is lost.

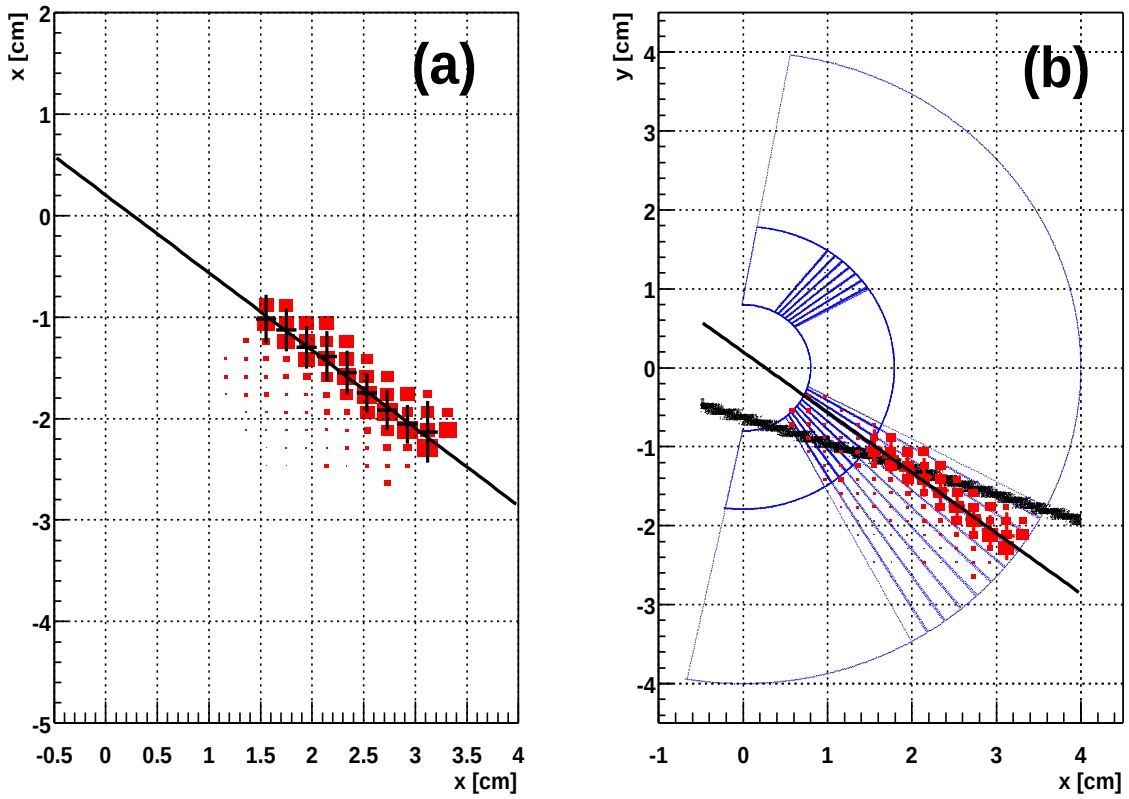

Figure 9: (a) A straight line fit to the inefficiency seen in the outer part of the detector (b) a comparison between the straight line fit (thin line) and the information from measurements taken at the time of the irradiation (thick line).

The performance of the inner and outer regions is compared in Figures 11(a)-(d). These show the charge measured in the diodes and in the routing lines, and the fraction of the total charge measured in the routing lines as a function of irradiation. This is shown for both the inner ((a) and (c)) and outer ((b) and (d)) regions. All data were collected with the detector biased at 300 V. The charge distributions in the diodes and the routing lines were fitted with a pseudo–Landau [1] to extract the most probable ADC value.

For the inner region, there is a pickup of about 4% in the routing lines. In the outer region the charge seen in the routing lines depends on the amount of underdepletion. For the zones of low irradiation, where the detector is still fully depleted at 300 V, there is just 5% seen in the routing lines. For the zones of high irradiation, where the detector is underdepleted, the fraction of charge seen in the routing lines rises to 20%. This extra charge loss is the reason for the additional inefficiency seen in the outer part of the detector. A 20% loss to the routing lines has also been observed in laboratory measurements of an irradiated 300 μm thick detector of identical design [10].

In the case of an n-on-n detector there is expected to be no charge spread, and no charge loss to the second metal layer [9].

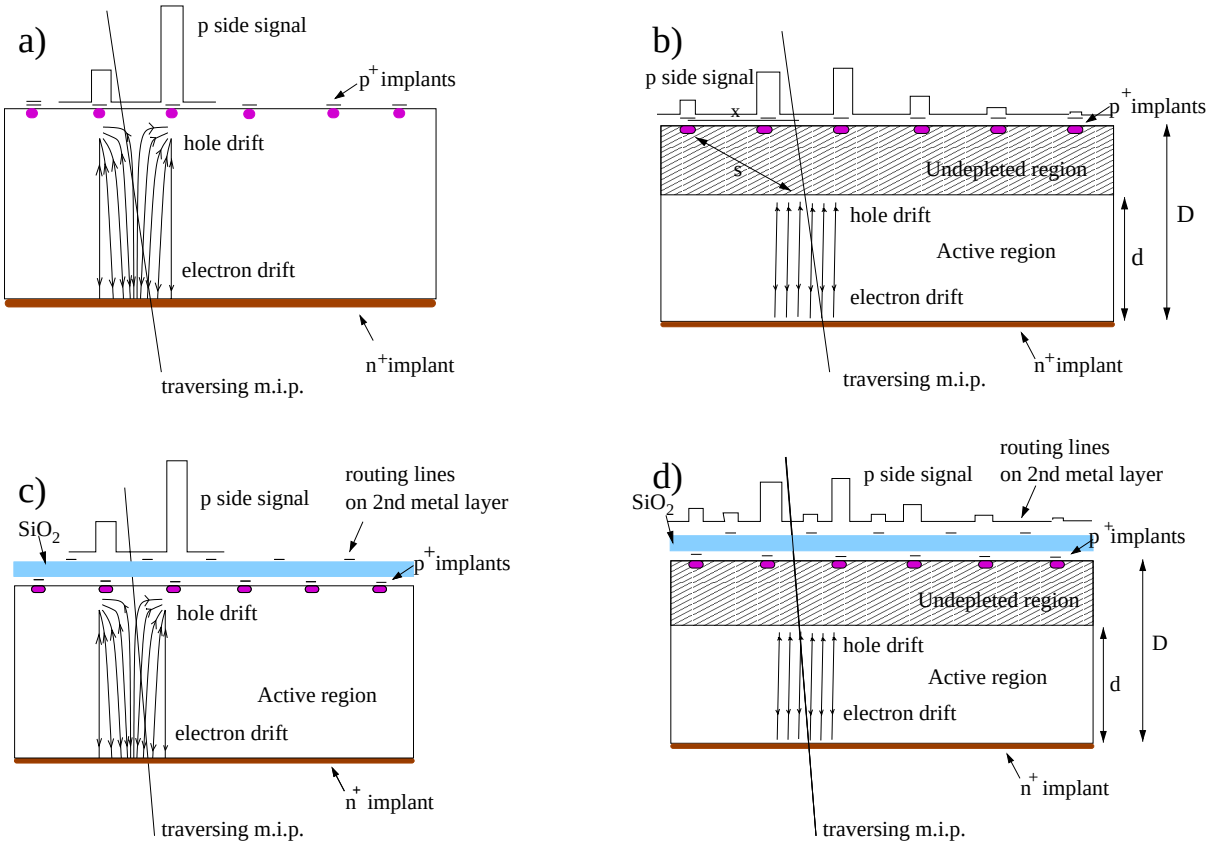

Figure 10: Sketches illustrating how charge is collected on the irradiated MICRON p-on-n detector for 4 scenarios: (a) inner region fully depleted, (b) inner region underdepleted, (c) outer region fully depleted, and (d) outer region underdepleted.

8 CCE measurement

When measuring the CCE the charge from 5 strips, plus the charge from the routing lines, about the intercept point of the track was summed. This was then fitted with a pseudo–Landau [1] for various voltage and irradiation levels. The result is shown in Figure 12. It can be seen that the maximum CCE, as defined by the 300 V measurement on the non-irradiated side, is reached after 300 V for a region of irradiation corresponding to $(1-2)\times10^{14}$ protons/cm^2. For the most irradiated region 93% of the maximum CCE is reached at 350 V.

The depletion voltage of the device may be determined from the points measured in Figure 12. A straight-line fit was performed to the data points that lay below 90% of the maximum CCE point. The depletion voltage was taken from the intercept point of this line with the level of the maximum CCE observed, this is shown in Figure 13. Note, that due to charge trapping effects, it may be necessary to significantly over-deplete heavily irradiated detector before the full charge is collected. The significant errors on the depletion voltage reflect the range of values that would be obtained from alternative strategies, such as taking the voltage at which 80% of the charge is collected. In Figure 13 the data is compared with the depletion voltage model described in Section 3.2 and may be seen to compare unfavourably for irradiations less than 6×10^{14} protons/cm^2. Recall that the model is based on tests of diodes, and that the depletion voltage was determined

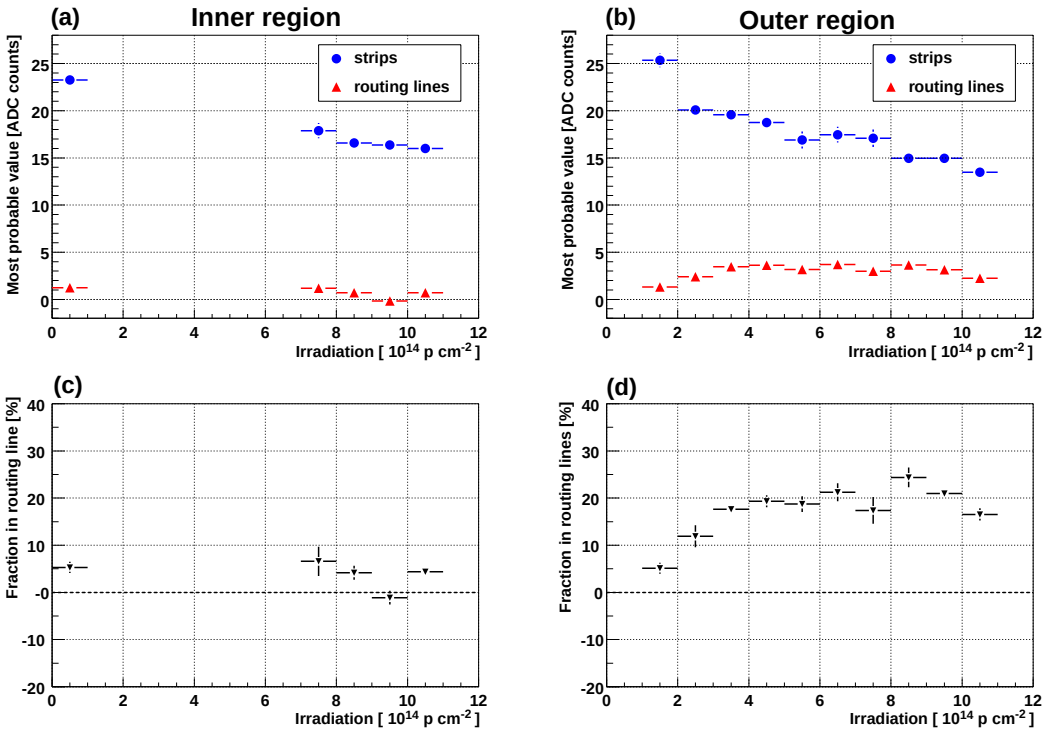

Figure 11: The amount of charge measured in the diodes and the routing lines ((a) and (b)), and the fraction in the routing lines ((c) and (d)) as a function of irradiation. The fraction in the routing line is defined as the charge in the routing lines divided by the sum of the charge in the routing lines and the strips. This is shown for the inner and outer regions. All data were collected at a bias voltage of 300 V.

from the behaviour of the capacitance with voltage of these samples.

The maximum CCE of the MICRON detector is 30.3 ADC counts when the routing lines are included. The non–irradiated timing station which is equipped with SCT128A electronics gives a maximum CCE of 58.5 ADC counts. For a fully depleted detector the CCE is proportional to the detector thickness. Therefore, the maximum CCE for the fully depleted MICRON detector is expected to be the maximum CCE from the timing station multiplied by the ratio of thicknesses of the MICRON to timing detector. The ratio of the thicknesses is $\frac{2}{3}$ so the expectation for the MICRON detector is 40 ADC counts. The 25% loss in charge is not understood and is much greater than the 5% gain variations of the SCT128A [11]. This loss is currently under investigation.

9 Efficiency measurement

For the efficiency measurement we look at the probability to reconstruct a cluster close to the track (200 μm) with a signal–to–noise of greater than 3, 5, and 10. A value of 5 is likely to be the one used to find clusters for the level–1 trigger at the startup of LHCb; this is expected to be lowered, as the radiation damage increases, to maintain the trigger efficiency [12].

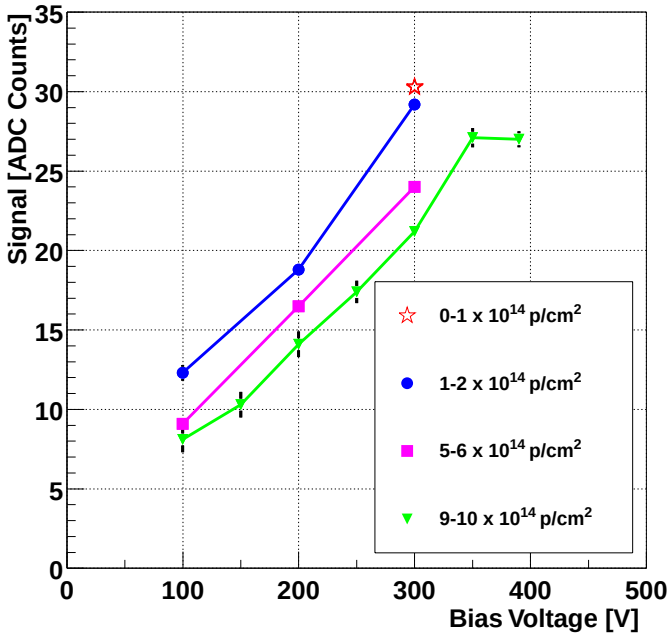

Figure 12: Charge collection efficiency as a function of depletion voltage for different irradiation levels.

9.1 Inner Region

The efficiency in the inner region as a function of depletion voltage is shown in Figure 14, for a mean irradiation of 9.5×10^{14} protons/cm^2. The efficiency reaches a maximum of 97% for voltages above 350 V for the whole irradiated inner region. At lower voltages it falls rapidly, due to a combination of the effects of charge loss and the spreading of the cluster over many strips. On the non–irradiated side of the detector the efficiency was $98.6 \pm 0.3\%$.

In both regions the probability of reconstructing a cluster given a random track position is 20%, 1.5% and $< 0.5\%$ for a signal–to–noise cut of 3, 5 and 10 respectively.

9.2 Outer Region

The efficiency of the outer region as a function of irradiation for the 3 signal–to–noise cuts is shown in Figure 15. The performance in the outer region is not as good as that in the inner region, due to the charge loss in the routing lines discussed in Section 7.1. A possible strategy to recover this charge is to add in the routing line charge to the cluster search algorithm in the outer region. However, including the routing lines in the algorithm would be difficult due to the low charge they pick up and the ambiguity with respect to the inner region.

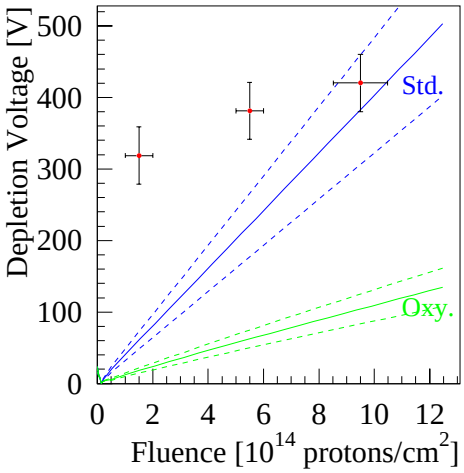

Figure 13: The depletion voltage with irradiation fluence is shown for the non–oxygenated test detector and compared with the expected performance for non–oxygenated and oxygenated diodes.

10 Cluster Shapes

As discussed in Section 5 the alignment of the system was not optimal. The poor quality of the alignment has prevented a measurement of the dependence of the resolution on irradiation and voltage. However, information on the detector resolution can be obtained from the study of the cluster shapes [1].

The analysis method was identical to that described in [1]. Only the finest pitch (24 μm $\leq$ pitch $<$ 40 μm) irradiated and non–irradiated inner regions were studied. The intercepted track positions as a function of R over these regions were approximately flat; therefore, the mean pitch was 34 μm. Data were only collected at a bias voltage of 300 V on the non–irradiated region ($< 1 \times 10^{14}$ protons/cm^2). Data were collected at voltages between 100 to 390 V on the irradiated region ($> 9 \times 10^{14}$ protons/cm^2).

Figures 16 (a) and (b) show the most probable values from the pseudo–Landau fits as a function of cluster extent for the non–irradiated and irradiated regions respectively. In Figure 16(b) only three voltage points are given for clarity. The distribution from the non–irradiated region is flat. For the irradiated region the charge collected increases as the cluster extent increases for the three voltage points shown. This is evidence that in the irradiated region of the detector the resolution would degrade due to the charge not being focused within two strips. This behaviour is consistent with that of a p–on–n detector which is both irradiated and underdepleted as described in Section 7.1. Furthermore, the spreading of the charge in an irradiated prototype detector of identical design has been observed in laboratory measurements [10].

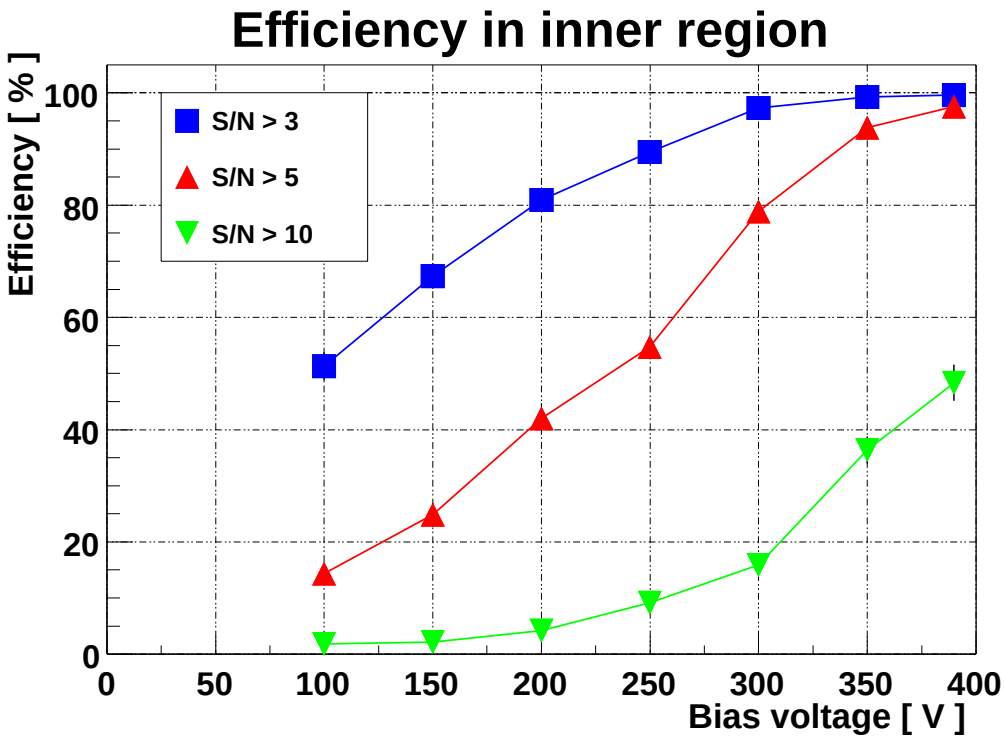

Figure 14: Efficiency, defined as the probability to reconstruct a cluster close to the traversing track, for three different signal–to–noise cuts, for the inner region of the detector. The mean irradiation level was 9.5×10^{14} protons/cm^2.

11 Signal–to–Noise performance

The SCT128A pulse shape when reading out the irradiated MICRON detector is reported in [11]. The maximum value of the signal recorded for the MICRON detector, when the routing lines are not included, was 27.1±2.6 ADC counts[3]. The common–mode suppressed noise measured on the strips was 1.76 ADC counts. Hence, the signal–to–noise ratio for the fully depleted detector was estimated to be 15.4 ± 1.5.

The evolution of the noise as a function of bias voltage was studied. Figure 17 shows the channels connected to the inner strips on the non–irradiated side of the detector and all channels on the irradiated side of the detector, for different voltages. Groups of unconnected channels are characterised by having equal raw and common–mode noise.

As the voltage was increased the noise behaviour remained stable until 350 V, apart from a small increase in common–mode contribution on the non–irradiated side of the detector. At 390 V the common–mode corrected noise increased to 6 ADC counts on the non–irradiated chip. There is also greater noise in alternate channels > 850 on the irradiated side as shown in Figure 18. Those with increased noise correspond to strips in the least irradiated part of the outer region (see Figure 2); those where the noise remains at a lower level are in the inner region which was irradiated to a high level. Similar behaviour for groups of channels with different irradiations was observed in the Liverpool

[3]The error is the systematic uncertainty associated with the choice of pseudo–Landau used to fit the charge distribution as discussed in [11]. The statistical uncertainties is negligible in comparison.

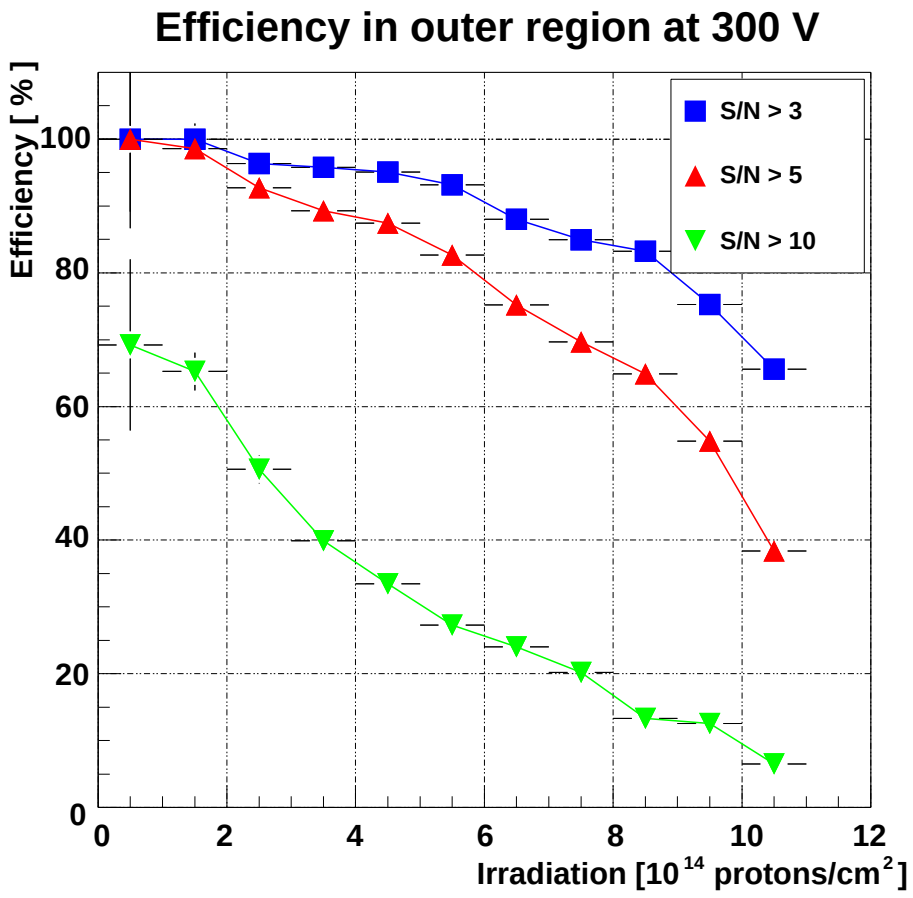

Figure 15: Efficiency measured at a bias voltage of 300V in the outer region of the detector, in different irradiation regions.

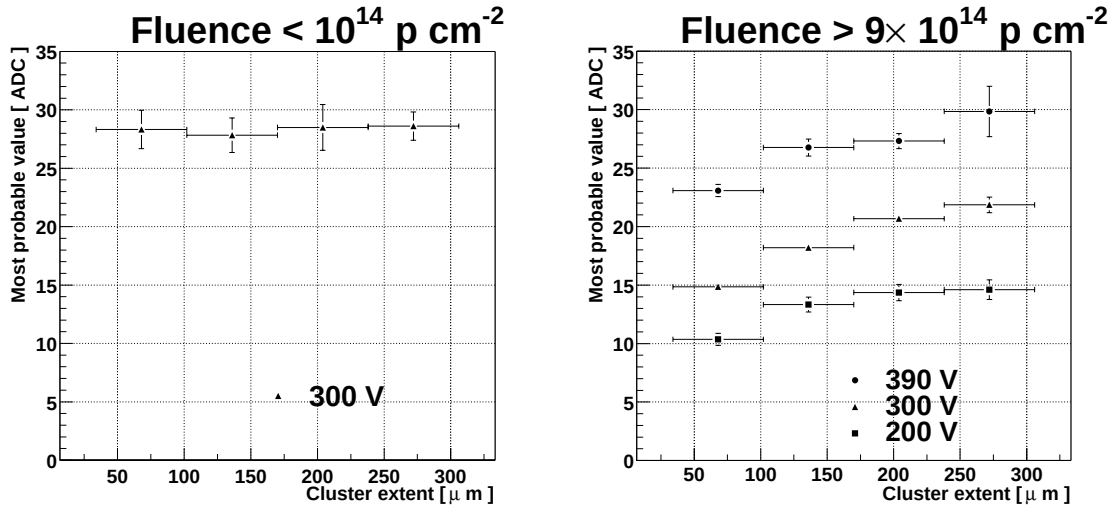

(a) (b)

Figure 16: The cluster extent at different irradiations: (a) fluence $< 10^{14}$ protons/cm^2 and (b) fluence $> 9 \times 10^{14}$ protons/cm^2.

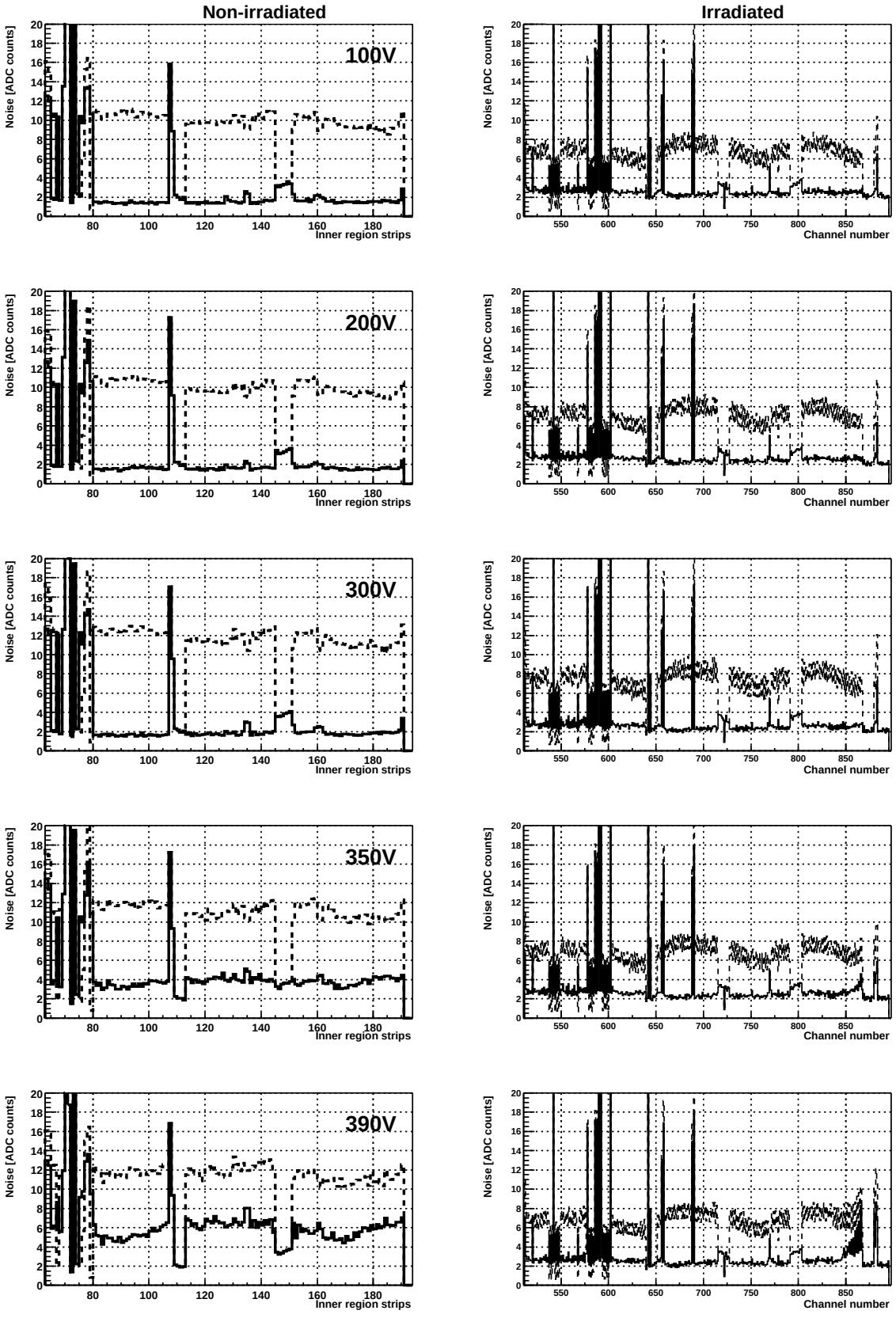

Figure 17: The raw (dashed) and common–mode corrected (solid) noise on the non–irradiated side (left) and irradiated side (right) for 5 different voltages.

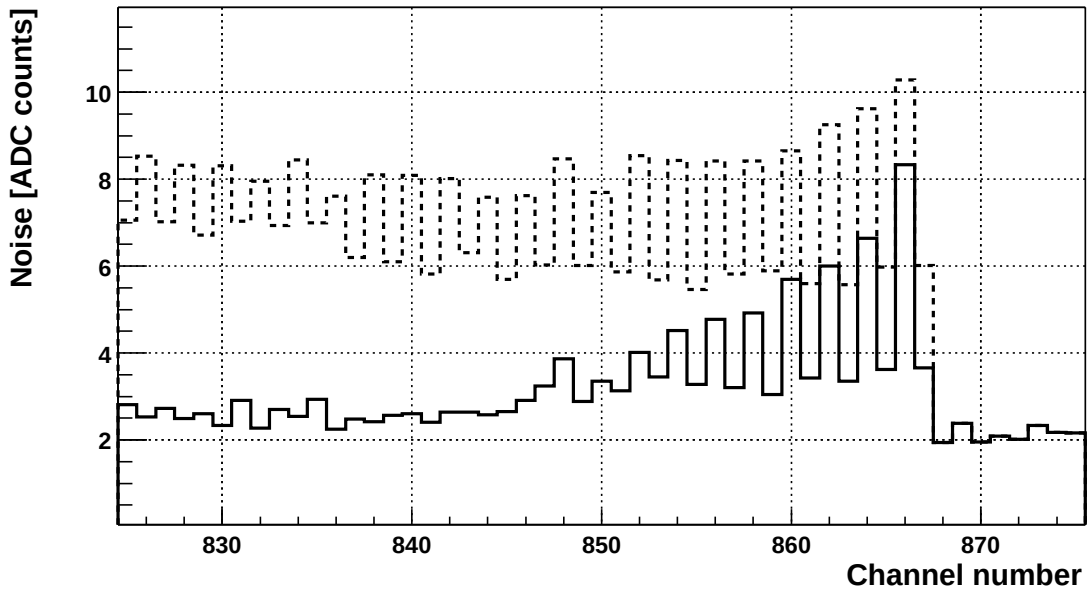

Figure 18: The raw (dashed) and common–mode corrected (solid) noise on the irradiated side at 390 V for channels 825 to 875. This plot corresponds to an expanded region of the bottom plot in the right–hand column of Figure 17.

Irradiation level [10^{14} protons/cm^2]	Equivalent LHCb years	Measured V_{dep}	Expected V_{dep}	
			Oxygenated Si	Standard Si
1.5	~ 1	320 V	20 V	65 V
5.5	~ 3	380 V	60 V	220 V
9.5	~ 5	420 V	110 V	400 V

Table 2: The measured values of V_{dep} for different irradiations compared to the expectation from the measurements of the ROSE collaboration for oxygenated and standard silicon.

laboratory test of a 300 μm thick detector of identical design [10].

This may be an indication of micro–discharge around the p^+ implants in a p–on–n detector. This phenomenon is discussed further in the conclusions given in Section 12.

12 Conclusions

A 200 μm thick p–on–n MICRON VELO PR-02 prototype ϕ detector has been irradiated non-uniformly up to levels of 10^{15} protons/cm^2 and tested with beams of minimum ionising particles, using LHC–speed SCT128A electronics.

In Table 2 the depletion voltages measured are given along with the expectations for standard and oxygenated silicon derived from the ROSE collaboration measurements which were reported in Section 3.2. Measurements for three different irradiations corresponding to nearly one, three and five years of LHCb running are given. The results are

worse than expected for a non–oxygenated detector in regions where the irradiation is less than 6×10^{14} protons/cm^2. The CCE agrees with the ROSE predictions at an irradiation of 9.5×10^{14} protons/cm^2. The best signal–to–noise for the MICRON detector, at full charge collection efficiency, was measured to be 15.4 ± 1.5.

The dangers of underdepleted p–on–n detectors with double metal readout have been observed. There was a loss of up to 20% of the charge in the outer region to the routing lines when the detector was underdepleted. Such a loss is recuperated in the CCE measurement due to the geometry of the MICRON ϕ detector. For a more complicated double–metal routing line geometries, such as the MICRON LHCb VELO PR–02 prototype R–measuring detector [4], such a procedure would be impossible. Even with the inclusion of the charge in the routing lines the maximum CCE of the fully depleted detector is 25% less than the expectation from other SCT128A equipped detectors [1].

The charge loss degrades the cluster–finding efficiency even when the detector is operated at 300 V in the outer region. Even in the inner region the efficiency is only 97% at the highest voltage and a S/N cut of 3 in the irradiated region. With such a performance in the LHCb VELO the present level–1 trigger algorithm, which searches for a triplet of hits in successive R–stations, the trigger efficiency would be degraded [12].

The focusing of the observed clusters was measured, and it was found that the clusters are unfocused due to underdepletion after irradiation. This is consistent with previous results for a p–on–n detector [9].

The noise behaviour was found to be quite stable up to 350 V. The noise increased in the least irradiated regions at this voltage which may be the result of micro–discharge. The micro–discharge noise is expected to be worse when the depletion region grows from the same side as the strips, and high fields can develop around the strips or p-stops. Hence, after irradiation, and when high voltages are applied, micro–discharge noise will be worse for an n-on-n design than a p-on-n design [13]. In the case of LHCb, where the irradiation is non-uniform, there is the risk in the p-on-n case that the depletion voltage, which needs to be applied to get the best efficiency from the irradiated part, will cause micro–discharge noise in the non-irradiated part. Conversely, in the n-on-n case the micro–discharge noise will appear for the irradiated region. However in the case of n-on-n detectors there are safety factors. We can still expect full efficiency and resolution when the voltage is slightly below the depletion voltage, so there is the option to tune the voltage to optimise the signal to noise. In addition the micro–discharge noise may be helped with the use of p-spray [14]. In the p-on-n case good operation can only be achieved at the highest voltage, so in the case of non-uniform irradiation micro–discharge noise poses more of a risk.

In summary there are at least four problems, not all of which are understood, with this p–on–n prototype:

- the loss of charge to routing lines and the spreading of charge when underdepleted,
- the possible increase in noise, due to micro–discharge, in the least irradiated regions when fully depleting the irradiated regions of the detector,
- the high depletion voltage for the detector at irradiations less than 6×10^{14} protons/cm^2 and,
- the CCE is 25% less than expectation.

The above findings compared to the tests of the n–on–n prototype [1] vindicate the choice of n–on–n detectors as the baseline sensor technology for the LHCb VELO.

Despite the caveats mentioned above this detectors performance was outstanding in one respect: the detector was collecting charge and reconstructing clusters even after an irradiation of 10^{15} protons/cm^2.

13 Acknowledgements

We would like to thank Lau Gatignon, Rolf Lindner and the staff of the CERN-PS accelerator for their support during the test-beam. We also very much appreciate the work of Angelo Gandi, Rui de Oliveira and Antonio Teixeira in the CERN Photomechanical workshops (EST-SM-CI), and Alan Honma and Enrico Chesi, also at CERN, for wire bonding and hybrid design. We are very grateful to Jean-Rene Moser and the Lausanne workshop. Thanks to Michael Moll for his assistance with the annealing studies.

References

[1] *Performance of an irradiated n–on–n Hamamatsu prototype VELO detector*, T. Bowcock et al., LHCb-2001-039.

[2] Further details are available at the URL http://www.ph.liv.ac.uk/lhcb/

[3] *VELO Technical Design Report*, LHCb collaboration, CERN LHCC 2001–010.

[4] *Detector Geometry - Vertex Locator test–beam software description*, C. Parkes, LHCb-2000-096.

[5] *SCTA - A rad-hard BiCMOS analogue readout ASIC for the ATLAS semiconductor tracker*, F. Anghinolfi *et. al.*, IEEE Transactions on Nuclear Sciences, Vol. 44, 1997.

[6] *Measurement of the Irradiation Profile at the PS Beam*, G. Casse *et. al.*, LHCb-2001-020.

[7] *Radiation Damage in Silicon Particle Detectors*, M. Moll, DESY-THESIS-1999-040. *Radiation Hardness of Silicon Detectors - a challenge from high-energy physics*, G. Lindstroem, M. Moll, E. Fretwurst, NIM A 426 (1999) 1.

[8] 3$^{\mathrm{RD}}$ *RD48 Status Report*, F. Lemeilleur *et. al.* CERN/LHCC 2000-009.

[9] Charge collection efficiency and resolution of an irradiated double sided silicon microstrip detector operated at cryogenic temperatures, P. Bartalini *et. al.*, NIM A 440 (2000) 17-37.

[10] *Characterisation of an inhomogeneously irradiated microstrip detectors using a fine spot infrared laser*, G. Casse *et al.*, LHCb-2001-053.

[11] *Performance of the SCT128A ASIC when reading out irradiated and non–irradiated VELO prototype detectors*, M. Charles *et. al.*, LHCb-2001-041.

[12] *Simulation of the vertex trigger preprocessor: Effects of noise on L1 performance*, P. Koppenburg, LHCb 99–003 TRIG.

[13] *A comparison of the performance of irradiated p-in-n and n-in-n silicon microstrip detectors read out with fast binary electronics*, P.P. Allport *et. al.*, NIM A 450 (2000) 297-306

[14] *Design optimisation of radiation-hard, double-sided, double-metal, AC-coupled silicon sensors*, T. Ohsugi *et. al.*, NIM A 436 (1999) 272-280